# Red, White & Blue: Identifying Recombination Loss Mechanisms in Perovskite Solar Cells

Sander Heester,[1] Lidón Gil-Escrig,[2] Federico Ventosinos,[3] Michele Sessolo,[2] Henk J. Bolink,[2] and L. Jan Anton Koster[1,*]

[1]*Zernike Institute for Advanced Materials, University of Groningen, Nijenborgh 3, 9747AG, Groningen, The Netherlands*
[2]*Instituto de Ciencia Molecular, Universidad de Valencia, C/Catedrático J.Beltrán 2, 46980, Paterna, Spain*
[3]*Instituto de Física del Litoral (IFIS-Litoral), CONICET-UNL, Güemes 3450, S3000GLN Santa Fe, Argentina*

(Received 16 December 2025; revised 21 April 2026; accepted 16 June 2026; published 14 July 2026)

Photovoltaics play a key role in the renewable energy transition, where perovskite solar cells stand out as one of the most promising with high-power conversion efficiencies, desirable characteristics, and great versatility. The efficiency of these cells is mainly limited by nonradiative recombination, whether at one of the interfaces between the perovskite layer and transport layers or within the bulk of the perovskite itself. However, it is difficult to probe which of these dominates the losses during operation, which complicates further improvements. Here we introduce and demonstrate a simple, inexpensive, and easy-to-integrate method for identification of the limiting aspect of perovskite solar cells under operating conditions in terms of recombination losses. We illuminate a device with red, blue, or white light, each absorbed differently depending on the position in the device. We show that, in perovskite solar cells, the diffusion length in the bulk is of secondary importance and rather the interfaces between layers dominate the charge carrier distributions, and thus light of different wavelengths will result in changing performance. Using the fill factor from the device characteristics for each case, we are able to identify whether the front or back interface of the cell limits the performance with nearly 97% accuracy. Finally, we apply this principle experimentally using a co-evaporated perovskite solar cell, where we show a decrease of nearly 5% in fill factor depending on the wavelength of light used.

DOI: 10.1103/g1cg-fnkn

Perovskite solar cells (PSCs) have attracted great interest in the past decade, evident from their rapid rise in power conversion efficiency (PCE) [1–3]. Perovskites show desirable properties such as strong optical absorption, long carrier diffusion lengths, and tunable bandgaps, making them suitable materials not only for single-junction applications but also for multijunction architectures such as tandem solar cells [4–12]. Much of the progress to date has been driven by novel fabrication techniques, improved processing methods, and optimized material compositions and combinations [13–24]. However, further improvements in device performance require more structured approaches, with increasing focus and efforts directed toward tuning and optimizing the charge transport layers (CTLs) and interface engineering [25–28]. Nonetheless, one of the main factors that limits the performance of current PSCs is nonradiative, trap-assisted recombination or Shockley-Read-Hall (SRH) recombination [29,30].

SRH recombination takes place both in the bulk of the perovskite and at the interfaces between the perovskite and CTLs, where recombination at the interfaces is often considered to contribute most to the recombination losses [31–35]. To mitigate these losses, it is essential to identify which part and which interface of the device truly limits the performance, in terms of nonradiative recombination losses, such that targeted efforts can be made to improve the overall PCE.

There are many reports and studies that focus on the identification and quantification of recombination processes in PSCs; however, a lot of these experimental reports are performed on just perovskite thin films [36–43]. Commonly used techniques are time-resolved photoluminescence imaging, photoluminescence quantum yield (PLQY), time-resolved microwave conductivity measurements or transient absorption spectroscopy to reveal the recombination dynamics [44–54]. While these methods provide valuable insight into the fundamental recombination mechanisms, they do not address the issue of

*Contact author: l.j.a.koster@rug.nl

which part, either one of the interfaces or the bulk of the perovskite, of the device dominates, whether the nonradiative recombination losses under operating conditions [at maximum power point (MPP) and under AM1.5 G illumination] and full device configuration.

In this work, we present a simple yet accurate method to probe the different SRH recombination channels in PSCs using light of different wavelengths and identify which dominates the losses under standard operating conditions. The method is easy to perform, inexpensive, and can be integrated into almost any existing experimental setup. It exploits the principle that light is absorbed differently in a PSC depending on the wavelength, selectively probing parts of the device and thereby trigger specific SRH recombination processes. We first show that in thin-film devices with CTLs, the bulk diffusion length is indeed very long, but despite this the charge carrier distribution is not uniform, in contrast to other photovoltaic technologies. We illustrate this with drift-diffusion modeling and show that the charge carrier distribution is dominated by the interfaces with the CTLs rather than by the bulk diffusion length. Next, we show the effect of using light of different wavelengths, which leads to different charge carrier generation profiles. Light in the red part of the spectrum generates carriers uniformly throughout the device, whereas light in the blue part of the spectrum primarily generates carriers at the front of the device. The contrast in fill factor (FF) for different light sources allows us to determine whether recombination at the front or the back interface is the dominant loss channel. We validate this by modeling a wide variety of PSCs, for which we have been able to identify the limiting interface in close to 97% of the cases using this method. Finally, we apply this principle experimentally with a co-evaporated *nip* PSC.

The bulk diffusion length is an important property in photovoltaics [55–57]. It quantifies the distance that charges can travel before recombining. It is especially crucial in silicon photovoltaics, where carriers often need to travel large distances before reaching the junction due to the thick absorber layer. Perovskites have exceptionally long bulk diffusion lengths, where the typical diffusion length is many times longer than the thickness of a PSC [58–60].

We can estimate the bulk diffusion length in a typical PSC by taking into account first-order recombination, where the lifetime in the bulk is given by [61]

$$\tau_{n,p} = (C_{n,p} N_{\mathrm{t,bulk}})^{-1}, \tag{1}$$

where $C_{n,p}$ are the capture coefficients of electrons and holes, respectively, and $N_{\mathrm{t,bulk}}$ is the density of trap states. The bulk diffusion length is given by

$$\lambda_{\mathrm{bulk}} = \sqrt{D\tau_{\mathrm{n,p}}}, \tag{2}$$

where $D$ is the diffusion coefficient. For a typical perovskite solar cell, the capture coefficients are $C_{n,p} = 1 \times 10^{-15}\ \mathrm{m^3\,s^{-1}}$, assuming the capture coefficients for electrons and holes are equal for simplicity. The bulk trap density is taken as $N_{\mathrm{t,bulk}} = 2.5 \times 10^{20}\ \mathrm{m^{-3}}$. The diffusion coefficient $D$ is given by the Einstein relation, $D = \mu k_b T/q$, where $\mu$ is the charge carrier mobility, $k_{\mathrm{B}}$ the Boltzmann constant, $T$ the temperature, and $q$ the elementary charge. Taking $\mu = 5 \times 10^{-4}\ \mathrm{m^2/Vs}$, which depends on the quality of the perovskite and, for example, the presence of grain boundaries, gives a diffusion coefficient of $D = 1.3 \times 10^{-5}\ \mathrm{m^2\,s^{-1}}$ [62]. This yields a carrier lifetime $\tau_{n,p} = 4\ \mu\mathrm{s}$ and a bulk diffusion length $\lambda_{\mathrm{bulk}} = 7\ \mu\mathrm{m}$, which is much larger than the typical PSC thickness of several hundred nanometers.

This seems to suggest that the position of charge carrier generation in the device will not matter, as carriers will just diffuse uniformly throughout the absorbing perovskite before recombining. However, this diffusion length, and by extension, the associated carrier transport and recombination dynamics are primarily relevant for single perovskite crystals or bare thin films [63]. They mostly reflect the amount of recombination in the bulk of the perovskite and the distance that charge carriers can travel before they recombine in the bulk of the material. Besides the fact that it does not provide any information on how fast the diffusion is, a thin-film PSC is not a bulk crystal and interfaces with the transport layers play a crucial role [64]. Additionally, the built-in electric field yields the needed asymmetry, required for a functional solar cell. From this it directly follows that the charge carrier profiles are asymmetric. In addition to this, light absorption and charge carrier generation in PSCs are also nonuniform and strongly depend on wavelength, device architecture and materials, affecting carrier distributions and dynamics, recombination processes, and consequently device performance [65–71].

To demonstrate these effects and the impact of light of different wavelengths on recombination mechanisms in more detail and for realistic PSCs, we employed 1D drift-diffusion simulations with SIMsalabim [72]. Simulations allow precise control over interface properties, recombination mechanisms, and illumination conditions.

To illustrate the nonuniformity of the charge carrier distribution, despite the long diffusion length in the bulk, we calculated the carrier densities of electrons and holes, as shown in Fig. 1, for progressively more complicated devices. It begins with a bare perovskite layer, and then different components are added sequentially until it becomes a realistic PSC, as shown in Fig. 1(a) and defined by the parameters in Table S1 in Supplemental Material [73]. Starting from a thick perovskite layer without transport layers and electrodes, thus without an electric field, extraction, and nonradiative recombination besides bulk recombination, Fig. 1(b) shows a uniform carrier profile. Adding perfectly passivated CTLs in Fig. 1(c), followed by electrodes in Fig. 1(d), results in a non-uniform distribution with a slight asymmetry. Extending this by

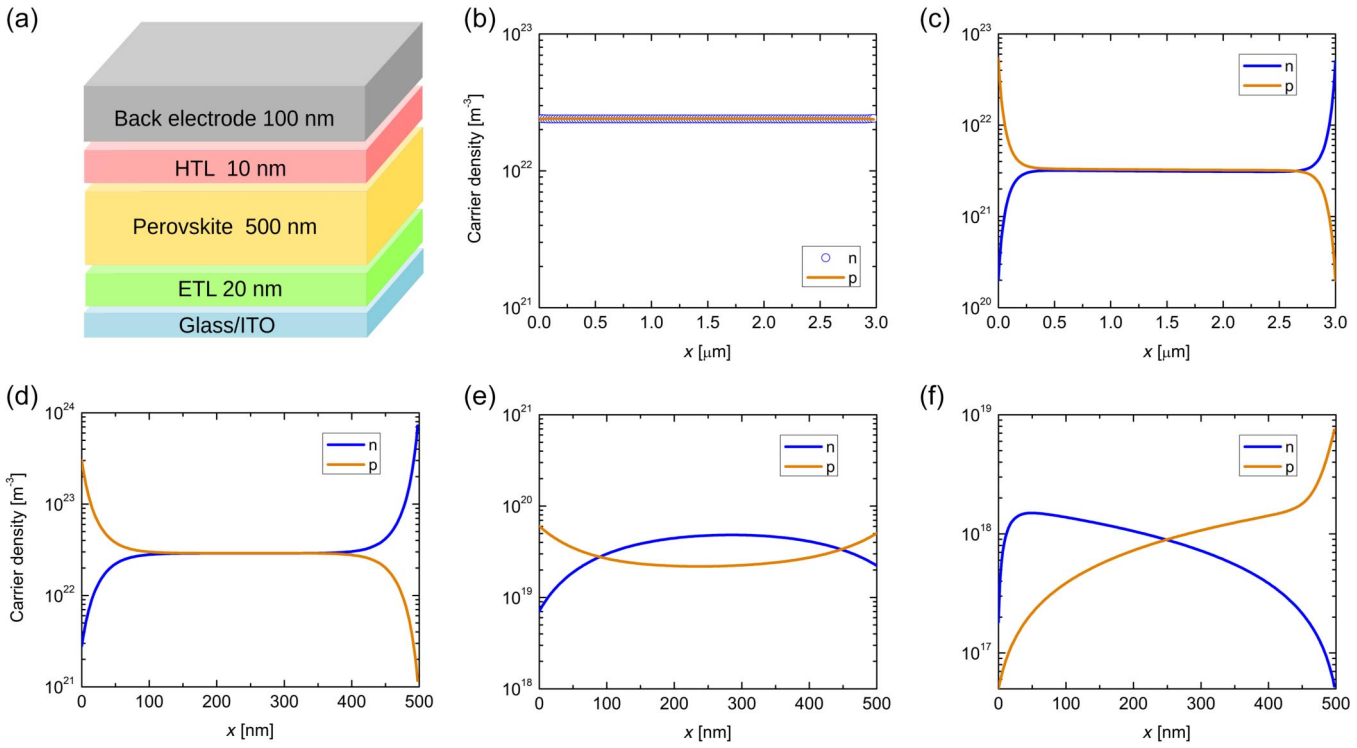


FIG. 1. (a) Schematic device structure of a typical thin-film PSC as defined in Table S1 in Supplemental Material [73]. Charge carrier profiles under standard AM1.5 G illumination for progressively more complicated devices: (b) bare perovskite layer without CTLs and electrodes, (c) perovskite with perfectly passivated CTLs but no electrodes, (d) perovskite with perfectly passivated CTLs and electrodes at open-circuit voltage, and a realistic PSC with CTLs, electrodes, and interface recombination under (e) open-circuit and (f) short-circuit conditions. While the carrier distribution is indeed uniform for a bare perovskite layer, for realistic solar cells the profiles for both electrons and holes are nonuniform, despite the long diffusion length in the bulk.

including the effects of interface recombination on either side, yields the nonuniform, asymmetric profiles in Figs. 1(e) and 1(f) under open-circuit and short-circuit conditions, respectively.

To probe the recombination processes in the device, we use light of different wavelengths, as these processes are directly related to the amount of generated charges available. Light absorption in perovskites is strongly wavelength dependent, characterized by the complex refractive index of the material [75,76]. Figure 2(a) shows the normalized charge generation profiles for blue, red, and white light in a PSC. Monochromatic light pulses were used here for the blue and red light, with the intensity adjusted to get the same short-circuit current density ($J_{sc}$) to ensure a fair comparison. Shorter wavelengths in the blue part of the spectrum are absorbed strongly at the front part of the device, whereas longer wavelengths in the red part of the spectrum are absorbed more uniformly throughout the device. The oscillatory behavior observed is due to interference caused by reflections at the interfaces and the back contact of the device.

Thus, depending on the wavelength, the majority of the electron-hole pairs are either generated near the front interface or more spread out throughout the device. From Fig. 2(a) it is clear that exposure of a PSC to blue light will result in a high excess carrier density near the front interface between the perovskite and the CTL. In that case, if there are both more carriers (both electrons and holes) and sufficient available trap states, recombination will be more substantial at that position in the device, which will affect the overall performance of the device and lead to a reduction of the FF. Figure 2(b) shows the current-voltage characteristics for the device as defined in Table S1 in Supplemental Material [73], under illumination with light of different wavelengths, where the FF decreases for shorter wavelengths [73].

To validate this principle, we simulated a wide variety of PSCs using SIMsalabim and analyzed the effect of the dominant recombination mechanisms and their positions on the FF. To achieve this, we randomly created $1 \times 10^6$ different devices by sampling the parameter space listed in Table S2 in Supplemental Material [73], resulting in a broad range of different PSCs. We varied layer thicknesses, permittivity, band alignment, effective density of states, charge carrier mobilities, trap densities, and capture coefficients for bulk and interface traps, as well as ion densities and mobilities [73]. The steady-state current-voltage (JV) curves for all simulated PSCs and the distribution of each parameter in the sampled space are shown in Figs. S3 and S4 in Supplemental Material [73] to

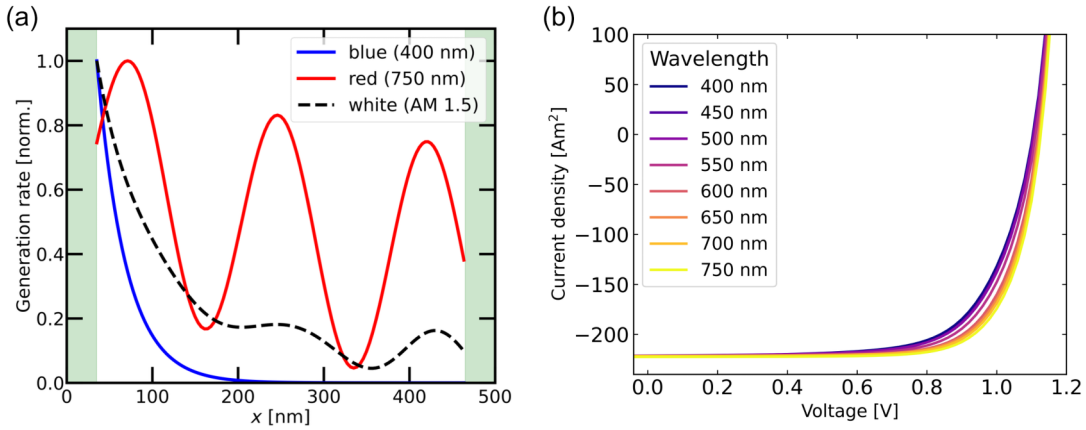


FIG. 2. (a) Normalized charge carrier generation profile in the PSC shown in Fig. 1(a) and as defined in Table S1 in Supplemental Material [73], calculated with SIMsalabim via the transfer matrix methodfor illumination with either red, white, or blue light [73,76]. Red light (750 nm) is absorbed throughout the device, while blue light (400 nm) is absorbed mainly in the first 150 nm of the device. The green areas represent the CTLs, in which the absorption is extremely low such that it can be neglected. (b) JV curves of the same PSC under illumination with light of different wavelengths, where the FF decreases for shorter wavelengths.

demonstrate that an extensive range of physically relevant PSCs has been sampled [73]. For each device, we extracted the FF under illumination with light of different wavelengths, while keeping the $J_{sc}$ constant per sample.

Figure 3(a) shows the FF as a function of the wavelength of the incoming light for the two scenarios, whether recombination at the front interface dominates the losses (blue circles) or not (red squares). As discussed before, light of shorter wavelengths is strongly absorbed near the front interface, creating a large amount of photogenerated carriers near this interface. This will lead to more recombination and thus a lower FF, provided that there are sufficient trap states. With increasing wavelength, the light gets absorbed more uniformly throughout the device, making it less influenced by the quality of the front interface, resulting in a higher fill factor. Thus, when recombination at the front interface dominates the losses, a significant decrease in FF is observed for shorter wavelengths compared to longer wavelengths, by 10% in this case. When recombination at the front interface is not dominant, the effects of illuminating with light of different wavelengths on the FF will be minimal, with even slightly higher FF values for shorter wavelengths. Even though blue light is absorbed strongly near the front interface, since there is very little recombination there, carriers will just diffuse through the device, resulting in a nearly

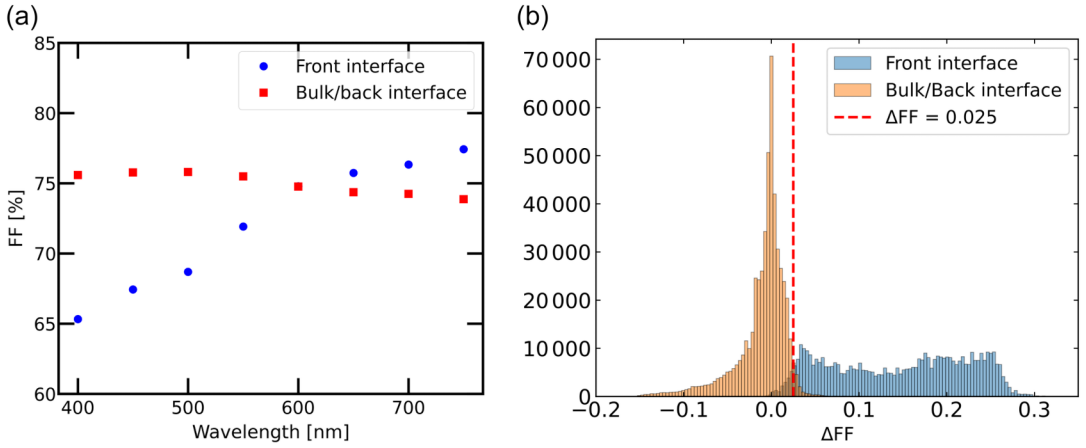


FIG. 3. (a) Simulated FF under illumination with light of different wavelengths for a representative PSC, when recombination at the front interface is the major loss mechanism (red squares) or recombination in the bulk in combination with the back interface dominates the losses (blue circles). In the case of the front interface, the FF significantly varies with the wavelength of the light used. The illumination intensity for each wavelength has been adjusted to ensure the same $J_{sc}$ for accurate comparison. (b) Histogram of the ΔFF of all simulated devices with the true classification of the dominant recombination mechanisms, where ΔFF is defined as the difference in FF between illumination with blue or red light. Using a classification threshold of 2.5% gives an accuracy of 97% in correctly identifying the dominant recombination loss mechanisms under operating conditions.

uniform FF as a function of the wavelength used. In this case, recombination at the back interface or in the perovskite bulk dominates the losses under operating conditions. Therefore, it is most likely the back interface that truly limits the device. As we have shown before, the diffusion length in the bulk is much longer than the perovskite thickness ($\lambda \gg L$), which results in minimal bulk recombination, making it an unlikely dominant loss mechanism. However, if under very specific circumstances the bulk diffusion length were to be much smaller than the perovskite thickness ($\lambda \ll L$), then recombination in the bulk would dominate the losses. Thus, measuring the FF for light of different wavelengths provides an effective an easy way to determine whether the front (FF drops under blue light) or back (FF remains constant) interface limits device performance due to nonradiative recombination losses.

To validate the accuracy of the method, we analyzed the contrast in FF between using blue and red light for all of the $1 \times 10^6$ simulated devices. To automatically assess this, we introduce the metric $\Delta\mathrm{FF} = \mathrm{FF}_{750} - \mathrm{FF}_{400}$, where $\mathrm{FF}_{750}$ is the FF using light of 750 nm and $\mathrm{FF}_{400}$ is the FF using light of 400 nm, where the classification threshold is $\Delta\mathrm{FF} = 2.5\%$. This means that if $\Delta\mathrm{FF}$ is larger than 2.5%, recombination at the front interface dominates the losses, and if $\Delta\mathrm{FF}$ is smaller than 2.5%, recombination at the back interface or in the bulk perovskite dominates the losses. Figure 3(b) shows a histogram of the $\Delta\mathrm{FF}$ for every device, classified by the true dominant recombination mechanism. Taking the classification threshold to be 2.5%, we achieve a 97% accuracy in identifying the dominant recombination mechanism under operating conditions (MPP and AM1.5 G illumination).

Finally, after demonstrating this effect in a controlled simulated environment, we applied it to experimental data for a co-evaporated *nip* PSC, where the perovskite is FACsPbIBr, the hole transport layer consists of a 10 nm *N*4, *N*4, *N*4″, *N*4″-tetra([1, 1′-biphenyl]-4-yl)-[1, 1′: 4′, 1″-terphenyl]-4, 4″-diamine layer and the electron transport layer (ETL) of a 10 nm $C_{60}$ layer. As contacts indium tin oxide combined with a thin layer of 2, 2′, 2″-(cyclopropane-1, 2, 3-triylidene)tris(2-(pcyanotetrafluorophenyl)acetonitrile) (CS90112) and covered with lithium fluoride (LiF) was used as the anode and silver (Ag) combined with a thin layer of bathocuroine was used as the cathode. The devices were first illuminated with a standard white light source. For the red and blue illumination, 440 and 730 nm LEDs were used, the spectra of which can be found in Fig. S2 in Supplemental Material [73]. The intensity was controlled to match approximately 0.1 sun equivalent, with comparable $J_{sc}$. Figure 4 shows the measured FF for each illumination source. Under blue light illumination, we observe a significant drop of close to 5% in FF, while for the red light, barely any change in FF is measured. The results are consistent with the simulated behavior as shown in Fig. 3(a) and identify the perovskite-ETL interface as the main recombination loss channel for this individual device.

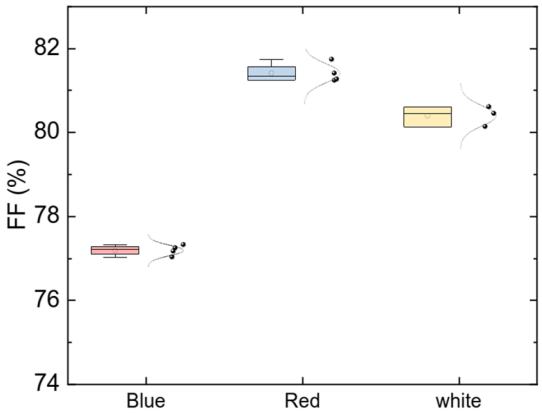


FIG. 4. The experimentally measured FF when the PSC is illuminated with either blue (440 nm), red (730 nm), or white light. A large difference, close to 5%, in FF is measured between blue and red light.

We have introduced a simple experimental method, that is both inexpensive and easy to integrate in almost any existing experimental setup, to identify the limiting interface in PSCs in terms of nonradiative recombination losses. We have elucidated the relevance of the diffusion length and the impact of interface recombination, which dominates the charge carrier distribution in PSCs, using drift-diffusion simulations. Furthermore, we have shown that illumination with light of different wavelengths allows us to probe different parts of the device, and specifically assess the interface between two layers. We demonstrate that there is a strong correlation between the limiting recombination pathway and the fill factor measured under blue light illumination, and that there are two distinct scenarios depending on whether the front or the back interface dominates the nonradiative recombination losses. Using this method, the limiting interface can be identified with nearly 97% accuracy. We applied this method to a wide bandgap PSC and identified the interface between the perovskite and the ETL to be the limiting part of that device in terms of nonradiative recombination losses.

This work was funded by the European Union; views and opinions expressed are, however, those of the authors only and do not necessarily reflect those of the European Union or CINEA; neither the European Union nor the granting authority can be held responsible for them. NEXUS project has received funding from Horizon Europe Research and Innovation Action programme under Grant Agreement No 101075330. M. S. acknowledges funding from the Comunitat Valenciana (CISEJI/2022/43).

S. H. contributed to conceptualization, formal analysis, investigation, methodology, software, validation, visualization, writing of the original draft, and review and editing

of the manuscript; F. V. contributed to investigation and review and editing of the manuscript; L. G. contributed to investigation and review and editing of the manuscript; M. S. contributed to investigation, supervision, and review and editing of the manuscript; H. J. B. contributed to funding acquisition, supervision, and review and editing of the manuscript; L. J. A. K. contributed to conceptualization, formal analysis, methodology, funding acquisition, supervision, and review and editing of the manuscript.

## DATA AVAILABILITY

The data that support the findings of this paper are available within the article and its supporting information, and was generated by numerical simulations with SIMsalabim and pySIMsalabim which are publicly available [72,77].


[1] M. A. Green, E. D. Dunlop, M. Yoshita, N. Kopidakis, K. Bothe, G. Siefer, D. Hinken, M. Rauer, J. Hohl-Ebinger, and X. Hao, *Solar cell efficiency tables (version 64)*, Prog. Photovoltaics **32**, 425 (2024).

[2] J. J. Yoo, G. Seo, M. R. Chua, T. G. Park, Y. Lu, F. Rotermund, Y.-K. Kim, C. S. Moon, N. J. Jeon, J.-P. Correa-Baena *et al.*, *Efficient perovskite solar cells via improved carrier management*, Nature (London) **590**, 587 (2021).

[3] S. Khatoon, S. K. Yadav, V. Chakravorty, J. Singh, R. B. Singh, M. S. Hasnain, and S. M. Hasnain, *Perovskite solar cell's efficiency, stability and scalability: A review*, Mater. Sci. Energy Technol. **6**, 437 (2023).

[4] S. D. Stranks, G. E. Eperon, G. Grancini, C. Menelaou, M. J. P. Alcocer, T. Leijtens, L. M. Herz, A. Petrozza, and H. J. Snaith, *Electron-hole diffusion lengths exceeding 1 micrometer in an organometal trihalide perovskite absorber*, Science **342**, 341 (2013).

[5] B. Chen, S.-W. Baek, Y. Hou, E. Aydin, M. De Bastiani, B. Scheffel, A. Proppe, Z. Huang, M. Wei, Y.-K. Wang *et al.*, *Enhanced optical path and electron diffusion length enable high-efficiency perovskite tandems*, Nat. Commun. **11**, 1257 (2020).

[6] G. E. Eperon, S. D. Stranks, C. Menelaou, M. B. Johnston, L. M. Herz, and H. J. Snaith, *Formamidinium lead trihalide: A broadly tunable perovskite for efficient planar heterojunction solar cells*, Energy Environ. Sci. **7**, 982 (2014).

[7] M. T. Hörantner, T. Leijtens, M. E. Ziffer, G. E. Eperon, M. G. Christoforo, M. D. McGehee, and H. J. Snaith, *The potential of multijunction perovskite solar cells*, ACS Energy Lett. **2**, 2506 (2017).

[8] X. Wu, B. Li, Z. Zhu, C.-C. Chueh, and A. K.-Y. Jen, *Designs from single junctions, heterojunctions to multi-junctions for high-performance perovskite solar cells*, Chem. Soc. Rev. **50**, 13090 (2021).

[9] H. Hu, S. X. An, Y. Li, S. Orooji, R. Singh, F. Schackmar, F. Laufer, Q. Jin, T. Feeney, A. Diercks *et al.*, *Triple-junction perovskite–perovskite–silicon solar cells with power conversion efficiency of 24.4%*, Energy Environ. Sci. **17**, 2800 (2024).

[10] S. Wang, W. Li, C. Yu, W. Shi, Q. Kang, F. Cao, K. Gao, L. Yang, B. Yang, J. Zhou *et al.*, *Flexible perovskite/silicon tandem solar cells with 33.6% efficiency*, Nature (London) **649**, 59 (2026).

[11] D. Wang, Z. Liu, Y. Qiao, Z. Jiang, P. Zhu, J. Zeng, W. Peng, Q. Lian, G. Qu, Y. Xu *et al.*, *Rigid molecules anchoring on* $NiO_x$ enable $>$ 26% *efficiency perovskite solar cells*, Joule **9** (2025).

[12] G. Yan, Y. Yuan, M. Kaba, and T. Kirchartz, *Visualizing performances losses of perovskite solar cells and modules: From laboratory to industrial scales*, Adv. Energy Mater. **15**, 2403706 (2025).

[13] Z. Saki, M. M. Byranvand, N. Taghavinia, M. Kedia, and M. Saliba, *Solution-processed perovskite thin-films: The journey from lab-to large-scale solar cells*, Energy Environ. Sci. **14**, 5690 (2021).

[14] J. Ávila, C. Momblona, P. P. Boix, M. Sessolo, and H. J. Bolink, *Vapor-deposited perovskites: The route to high-performance solar cell production?*, Joule **1**, 431 (2017).

[15] M. Saliba, T. Matsui, J.-Y. Seo, K. Domanski, J.-P. Correa-Baena, M. K. Nazeeruddin, S. M. Zakeeruddin, W. Tress, A. Abate, A. Hagfeldt *et al.*, *Cesium-containing triple cation perovskite solar cells: Improved stability, reproducibility and high efficiency*, Energy Environ. Sci. **9**, 1989 (2016).

[16] Y. Zhang, Y. Liu, and S. Liu, *Composition engineering of perovskite single crystals for high-performance optoelectronics*, Adv. Funct. Mater. **33**, 2210335 (2023).

[17] Y. Yao, C. Cheng, C. Zhang, H. Hu, K. Wang, and S. De Wolf, *Organic hole-transport layers for efficient, stable, and scalable inverted perovskite solar cells*, Adv. Mater. **34**, 2203794 (2022).

[18] W. Chi and S. K. Banerjee, *Stability improvement of perovskite solar cells by compositional and interfacial engineering*, Chem. Mater. **33**, 1540 (2021).

[19] J. Zhang, B. Liu, Z. Liu, J. Wu, S. Arnold, H. Shi, T. Osterrieder, J. A. Hauch, Z. Wu, J. Luo *et al.*, *Optimizing perovskite thin-film parameter spaces with machine learning-guided robotic platform for high-performance perovskite solar cells*, Adv. Energy Mater. **13**, 2302594 (2023).

[20] X. Tang, C. Yang, Y. Xu, J. Xia, B. Li, M. Li, Y. Zhou, L. Jiang, H. Liu, K. Ma *et al.*, *Enhancing the efficiency and stability of perovskite solar cells via a polymer heterointerface bridge*, Nat. Photonics **19**, 701 (2025).

[21] A. Diercks, S. Chozas-Barrientos, L. Gil-Escrig, F. Ventosinos, I. Gomar-Fernández, C. Roldán-Carmona, N. Rodkey, T. Zhao, J. Petermann, M. Senno *et al.*, *Close-space sublimation as a versatile deposition process for efficient perovskite silicon tandem solar cells*, Nat. Energy 1 (2026).

[22] Y. Zhang, Y. Liu, Z. Zhao, T. Kong, W. Chen, W. Liu, Y. Rong, and D. Bi, *Reduction of nonradiative recombination at perovskite/*$C_{60}$ *interface in inverted perovskite solar cells*, Adv. Mater. **37**, 2500501 (2025).

[23] J. Wang, L. Bi, Q. Fu, and A. K.-Y. Jen, *Methods for passivating defects of perovskite for inverted perovskite*

*solar cells and modules*, Adv. Energy Mater. **14**, 2401414 (2024).

[24] B. Jo, W. Chen, and H. S. Jung, *Comprehensive review of advances in machine-learning-driven optimization and characterization of perovskite materials for photovoltaic devices*, J. Energy Chem. **101**, 298 (2025).

[25] F. H. Isikgor, S. Zhumagali, L. V. T. Merino, M. De Bastiani, I. McCulloch, and S. De Wolf, *Molecular engineering of contact interfaces for high-performance perovskite solar cells*, Nat. Rev. Mater. **8**, 89 (2023).

[26] V. M. Le Corre, M. Stolterfoht, L. Perdigón Toro, M. Feuerstein, C. Wolff, L. Gil-Escrig, H. J. Bolink, D. Neher, and L. J. A. Koster, *Charge transport layers limiting the efficiency of perovskite solar cells: How to optimize conductivity, doping, and thickness*, ACS Appl. Energy Mater. **2**, 6280 (2019).

[27] W. Zhang, X. Guo, Z. Cui, H. Yuan, Y. Li, W. Li, X. Li, and J. Fang, *Strategies for improving efficiency and stability of inverted perovskite solar cells*, Adv. Mater. **36**, 2311025 (2024).

[28] P. Chen, Y. Xiao, J. Hu, S. Li, D. Luo, R. Su, P. Caprioglio, P. Kaienburg, X. Jia, N. Chen *et al.*, *Multifunctional ytterbium oxide buffer for perovskite solar cells*, Nature (London) **625**, 516 (2024).

[29] C. M. Wolff, P. Caprioglio, M. Stolterfoht, and D. Neher, *Nonradiative recombination in perovskite solar cells: The role of interfaces*, Adv. Mater. **31**, 1902762 (2019).

[30] P. Chen, Y. Bai, and L. Wang, *Minimizing voltage losses in perovskite solar cells*, Small Struct. **2**, 2000050 (2021).

[31] W. Tress, N. Marinova, O. Inganäs, M. K. Nazeeruddin, S. M. Zakeeruddin, and M. Graetzel, *Predicting the open-circuit voltage of* $CH_3NH_3PbI_3$ *perovskite solar cells using electroluminescence and photovoltaic quantum efficiency spectra: The role of radiative and nonradiative recombination*, Adv. Energy Mater. **5**, 1400812 (2015).

[32] T. S. Sherkar, C. Momblona, L. Gil-Escrig, J. Ávila, M. Sessolo, H. J. Bolink, and L. J. A. Koster, *Recombination in perovskite solar cells: Significance of grain boundaries, interface traps, and defect ions*, ACS Energy Lett. **2**, 1214 (2017).

[33] J. Warby, F. Zu, S. Zeiske, E. Gutierrez-Partida, L. Frohloff, S. Kahmann, K. Frohna, E. Mosconi, E. Radicchi, F. Lang *et al.*, *Understanding performance limiting interfacial recombination in pin perovskite solar cells*, Adv. Energy Mater. **12**, 2103567 (2022).

[34] F. Ye, S. Zhang, J. Warby, J. Wu, E. Gutierrez-Partida, F. Lang, S. Shah, E. Saglamkaya, B. Sun, F. Zu *et al.*, *Overcoming* $C_{60}$*-induced interfacial recombination in inverted perovskite solar cells by electron-transporting carborane*, Nat. Commun. **13**, 7454 (2022).

[35] R. D. Adhikari, M. J. Patel, H. Baishya, D. Yadav, M. Kalita, M. Alam, and P. K. Iyer, *Decoding recombination dynamics in perovskite solar cells: An in-depth critical review*, Chem. Soc. Rev. **54**, 3962 (2025).

[36] M. J. Trimpl, A. D. Wright, K. Schutt, L. R. V. Buizza, Z. Wang, M. B. Johnston, H. J. Snaith, P. Müller-Buschbaum, and L. M. Herz, *Charge-carrier trapping and radiative recombination in metal halide perovskite semiconductors*, Adv. Funct. Mater. **30**, 2004312 (2020).

[37] H.-S. Duan, H. Zhou, Q. Chen, P. Sun, S. Luo, T.-B. Song, B. Bob, and Y. Yang, *The identification and characterization of defect states in hybrid organic–inorganic perovskite photovoltaics*, Phys. Chem. Chem. Phys. **17**, 112 (2015).

[38] D. J. Keeble, J. Wiktor, S. K. Pathak, L. J. Phillips, M. Dickmann, K. Durose, H. J. Snaith, and W. Egger, *Identification of lead vacancy defects in lead halide perovskites*, Nat. Commun. **12**, 5566 (2021).

[39] X. Chen, P. V. Kamat, C. Janáky, and G. F. Samu, *Charge transfer kinetics in halide perovskites: On the constraints of time-resolved spectroscopy measurements*, ACS Energy Lett. **9**, 3187 (2024).

[40] J. Lim, M. Kober-Czerny, Y.-H. Lin, J. M. Ball, N. Sakai, E. A. Duijnstee, M. J. Hong, J. G. Labram, B. Wenger, and H. J. Snaith, *Long-range charge carrier mobility in metal halide perovskite thin-films and single crystals via transient photo-conductivity*, Nat. Commun. **13**, 4201 (2022).

[41] M. Kaiser, Y. Li, S. Gharibzadeh, B. S. Richards, U. W. Paetzold, and I. A. Howard, *Charge carrier and exciton dynamics in perovskites revealed by time-integrated photoluminescence after double-pulse excitation*, Adv. Mater. Technol. **7**, 2200152 (2022).

[42] C. Wang, G. Li, H. Cui, Y. Ge, S. Fu, H. Guan, S. Zhou, X. Hu, W. Shao, P. Jia *et al.*, *Reconstruction of the buried interface of triple-halide wide-bandgap perovskite for all-perovskite tandems*, Adv. Mater. **37**, 2502450 (2025).

[43] D. Guo, A. R. Bowman, S. Gorgon, C. Cho, Y.-K. Jung, J. Zhao, L. Dai, J. Park, K. M. Yeom, S. Nagane *et al.*, *Modulating non-radiative recombination related to shallow traps in halide perovskites*, Appl. Phys. Rev. **13**, 011419 (2026).

[44] F. Staub, H. Hempel, J.-C. Hebig, J. Mock, U. W. Paetzold, U. Rau, T. Unold, and T. Kirchartz, *Beyond bulk lifetimes: Insights into lead halide perovskite films from time-resolved photoluminescence*, Phys. Rev. Appl. **6**, 044017 (2016).

[45] K. P. Goetz, A. D. Taylor, F. Paulus, and Y. Vaynzof, *Shining light on the photoluminescence properties of metal halide perovskites*, Adv. Funct. Mater. **30**, 1910004 (2020).

[46] S. Cacovich, G. Vidon, M. Degani, M. Legrand, L. Gouda, J.-B. Puel, Y. Vaynzof, J.-F. Guillemoles, D. Ory, and G. Grancini, *Imaging and quantifying non-radiative losses at 23% efficient inverted perovskite solar cells interfaces*, Nat. Commun. **13**, 2868 (2022).

[47] T. Kirchartz, J. A. Márquez, M. Stolterfoht, and T. Unold, *Photoluminescence-based characterization of halide perovskites for photovoltaics*, Adv. Energy Mater. **10**, 1904134 (2020).

[48] J. Liu, H. Bì, L. Wang, Q. Shen, and S. Hayase, *Photoluminescence quantum yield in perovskite solar cells: Probing interface recombination and efficiency limits*, Solar RRL **9**, 202500409 (2025).

[49] G. O. Odunmbaku, S. Chen, B. Guo, Y. Zhou, N. A. N. Ouedraogo, Y. Zheng, J. Li, M. Li, and K. Sun, *Recombination pathways in perovskite solar cells*, Adv. Mater. Interfaces **9**, 2102137 (2022).

[50] J. Zhao, L. M. van der Poll, S. L. Looman, J. Yan, J. Thieme, B. Ibrahim, and T. J. Savenije, *Long-lived charge extraction in CsMAFA-based perovskites in n-i-p and p-i-n structures*, ACS Energy Lett. **9**, 2456 (2024).

[51] C. M. Wolff, S. A. Bourelle, L. Q. Phuong, J. Kurpiers, S. Feldmann, P. Caprioglio, J. A. Marquez, J. Wolansky, T. Unold, M. Stolterfoht *et al.*, *Orders of recombination in complete perovskite solar cells–linking time-resolved and steady-state measurements*, Adv. Energy Mater. **11**, 2101823 (2021).

[52] Y. Gao, J. Liu, F. H. Isikgor, M. Wang, J. I. Khan, S. De Wolf, and F. Laquai, *Probing ultrafast interfacial carrier dynamics in metal halide perovskite films and devices by transient reflection spectroscopy*, ACS Appl. Mater. Interfaces **14**, 34281 (2022).

[53] Q. Huang, W. Meng, Z. Yuan, H. Li, F. Huang, and N. Li, *Decoding charge recombination and extraction at perovskite interfaces with transient photoluminescence*, Small Methods **9**, 2500396 (2025).

[54] M. Simmonds, Y. Duan, M. F. Vasquez-Montoya, R. W. MacQueen, V. M. Le Corre, E. Unger, and T. Kirchartz, *Quantifying evolving defect parameters in metal halide perovskites via the measurement and modeling of power-dependent transient photoluminescence*, Adv. Energy Mater. **16**, e04811 (2026).

[55] A. Kitai, *Principles of Solar Cells, LEDs and Diodes: The Role of the PN Junction* (John Wiley & Sons, New York, 2011).

[56] G. Xing, N. Mathews, S. Sun, S. S. Lim, Y. M. Lam, M. Grätzel, S. Mhaisalkar, and T. C. Sum, *Long-range balanced electron-and hole-transport lengths in organic-inorganic* $CH_3NH_3PbI_3$, Science **342**, 344 (2013).

[57] T. Fuyuki, H. Kondo, T. Yamazaki, Y. Takahashi, and Y. Uraoka, *Photographic surveying of minority carrier diffusion length in polycrystalline silicon solar cells by electroluminescence*, Appl. Phys. Lett. **86**, 262108 (2005).

[58] A. A. Zhumekenov, M. I. Saidaminov, M. A. Haque, E. Alarousu, S. P. Sarmah, B. Murali, I. Dursun, X.-H. Miao, A. L. Abdelhady, T. Wu *et al.*, *Formamidinium lead halide perovskite crystals with unprecedented long carrier dynamics and diffusion length*, ACS Energy Lett. **1**, 32 (2016).

[59] Q. Dong, Y. Fang, Y. Shao, P. Mulligan, J. Qiu, L. Cao, and J. Huang, *Electron-hole diffusion lengths* $> 175$ μm *in solution-grown* $CH_3NH_3PbI_3$ *single crystals*, Science **347**, 967 (2015).

[60] B. Turedi, M. N. Lintangpradipto, O. J. Sandberg, A. Yazmaciyan, G. J. Matt, A. Y. Alsalloum, K. Almasabi, K. Sakhatskyi, S. Yakunin, X. Zheng *et al.*, *Single-crystal perovskite solar cells exhibit close to half a millimeter electron-diffusion length*, Adv. Mater. **34**, 2202390 (2022).

[61] S. Selberherr, *Analysis and Simulation of Semiconductor Devices* (Springer Science & Business Media, Vienna, Austria, 1984).

[62] C. Cho, S. Feldmann, K. M. Yeom, Y.-W. Jang, S. Kahmann, J.-Y. Huang, T. C.-J. Yang, M. N. T. Khayyat, Y.-R. Wu, M. Choi *et al.*, *Efficient vertical charge transport in polycrystalline halide perovskites revealed by four-dimensional tracking of charge carriers*, Nat. Mater. **21**, 1388 (2022).

[63] Y. Yuan, G. Yan, S. Akel, U. Rau, and T. Kirchartz, *Deriving mobility-lifetime products in halide perovskite films from spectrally and time-resolved photoluminescence*, Sci. Adv. **11**, eadt1171 (2025).

[64] S. Akel, A. Kulkarni, U. Rau, and T. Kirchartz, *Relevance of long diffusion lengths for efficient halide perovskite solar cells*, PRX Energy **2**, 013004 (2023).

[65] F. Berry, R. Mermet-Lyaudoz, J. M. Cuevas Davila, D. A. Djemmah, H. S. Nguyen, C. Seassal, E. Fourmond, C. Chevalier, M. Amara, and E. Drouard, *Light management in perovskite photovoltaic solar cells: A perspective*, Adv. Energy Mater. **12**, 2200505 (2022).

[66] G. F. Burkhard, E. T. Hoke, and M. D. McGehee, *Accounting for interference, scattering, and electrode absorption to make accurate internal quantum efficiency measurements in organic and other thin solar cells*, Adv. Mater. **22**, 3293 (2010).

[67] J. M. Ball, S. D. Stranks, M. T. Hörantner, S. Hüttner, W. Zhang, E. J. Crossland, I. Ramirez, M. Riede, M. B. Johnston, R. H. Friend *et al.*, *Optical properties and limiting photocurrent of thin-film perovskite solar cells*, Energy Environ. Sci. **8**, 602 (2015).

[68] B. Nath, P. C. Ramamurthy, D. R. Mahapatra, and G. Hegde, *Unveiling the wavelength-dependent performance and photodegradation analysis of perovskite solar cells*, ACS Appl. Energy Mater. **8**, 922 (2025).

[69] J. Henzel, K. Bakker, S. Veenstra, O. Isabella, L. Mazzarella, A. Weeber, and M. Theelen, *The impact of low-intensity illumination on the reverse bias behavior of perovskite solar cells*, J. Mater. Chem. A **13**, 31755 (2025).

[70] J. Hieulle, A. Krishna, A. Boziki, J.-N. Audinot, M. U. Farooq, J. F. Machado, M. Mladenović, H. Phirke, A. Singh, T. Wirtz *et al.*, *Understanding and decoupling the role of wavelength and defects in light-induced degradation of metal-halide perovskites*, Energy Environ. Sci. **17**, 284 (2024).

[71] L. Yue, B. Yan, M. Attridge, and Z. Wang, *Light absorption in perovskite solar cell: Fundamentals and plasmonic enhancement of infrared band absorption*, Sol. Energy **124**, 143 (2016).

[72] M. Koopmans, V. M. Le Corre, and L. J. A. Koster, *SIMsalabim: An open-source drift-diffusion simulator for semiconductor devices*, J. Open Source Software **7**, 3727 (2022).

[73] See Supplemental Material at http://link.aps.org/supplemental/10.1103/g1cg-fnkn, in which Ref. [74] is cited, for additional details and supporting tables and figures.

[74] C. A. Gueymard, D. Myers, and K. Emery, *Proposed reference irradiance spectra for solar energy systems testing*, Sol. Energy **73**, 443 (2002).

[75] P. Loper, M. Stuckelberger, B. Niesen, J. Werner, M. Filipic, S.-J. Moon, J.-H. Yum, M. Topic, S. De Wolf, and C. Ballif, *Complex refractive index spectra of* $CH_3NH_3PbI_3$ *perovskite thin films determined by spectroscopic ellipsometry and spectrophotometry*, J. Phys. Chem. Lett. **6**, 66 (2015).

[76] J. Werner, G. Nogay, F. Sahli, T. C.-J. Yang, M. Brauninger, G. Christmann, A. Walter, B. A. Kamino, P. Fiala, P. Loper *et al.*, *Complex refractive indices of cesium–formamidinium-based mixed-halide perovskites with optical band gaps from 1.5 to 1.8 eV*, ACS Energy Lett. **3**, 742 (2018).

[77] S. Heester, F. D. Elhorst, P. M. Fernandez, V. M. Le Corre, M. Koopmans, and L. J. Koster, *pySIMsalabim: A Python package to extend drift-diffusion modelling with SIMsalabim*, Comput. Phys. Commun. **323**, 110096 (2026).